

PCA-based filtering of temperature effect on impedance monitoring in prestressed tendon anchorage

Thanh-Canh Huynh^a, Ngoc-Loi Dang^b and Jeong-Tae Kim^{*}

Department of Ocean Engineering, Pukyong National University,
599-1 Daeyeon 3-dong, Nam-gu, Busan 608-737, Republic of Korea

(Received October 16, 2017, Revised April 8, 2018, Accepted April 28, 2018)

Abstract. For the long-term structural health monitoring of civil structures, the effect of ambient temperature variation has been regarded as one of the critical issues. In this study, a principal component analysis (PCA)-based algorithm is proposed to filter out temperature effects on electromechanical impedance (EMI) monitoring of prestressed tendon anchorages. Firstly, the EMI monitoring via a piezoelectric interface device is described for prestress-loss detection in the tendon anchorage system. Secondly, the PCA-based temperature filtering algorithm tailored to the EMI monitoring of the prestressed tendon anchorage is outlined. The proposed algorithm utilizes the damage-sensitive features obtained from sub-ranges of the EMI data to establish the PCA-based filter model. Finally, the feasibility of the PCA-based algorithm is experimentally evaluated by distinguishing temperature changes from prestress-loss events in a prestressed concrete girder. The accuracy of the prestress-loss detection results is discussed with respect to the EMI features before and after the temperature filtering.

Keywords: electromechanical impedance; impedance monitoring; temperature effect; temperature filtering; principal component analysis; prestressed tendon anchorage; prestress-loss

1. Introduction

The damage detection in structural systems using the impedance-based technique has received significant attention in recent years. To detect structural changes, the impedance-based method utilizes the electromechanical impedance (EMI) signals sensed by piezoceramic patches attached to the host structure. Various experimental and numerical works conducted on many types of civil infrastructures have demonstrated the potential of the method in the area of structural health monitoring (SHM) (Ayres *et al.* 1998, Soh *et al.* 2000, Park *et al.* 2003, Kim *et al.* 2010, Yang *et al.* 2008, Ho *et al.* 2012, Hu *et al.* 2014, Ho *et al.* 2014, Kim *et al.* 2014, Wang *et al.* 2016, Nguyen *et al.* 2017, Zahedi and Huang 2017, Ryu *et al.* 2017). By utilizing the promising properties of the piezoelectric materials (e.g., PZT), the impedance-based technique offers unique advantages. First, the technique can be easily applied to complex structures since it is non-model based. Second, the technique uses piezoelectric sensors which are commercially available at a low cost, typically less than \$10. Third, the technique using the high-frequency responses is very sensitive to minor incipient damage and less sensitive to operational vibrations of a monitored structure. Finally, the technique is very suitable for autonomous and real-time SHM implementations since requirements for data

processing are minimal (Soh *et al.* 2012, Huynh *et al.* 2017).

Despite the above-mentioned potentials, challenges still exist against the field application of the technique. A critical one is the effect of ambient temperature changes on the EMI responses that could cause false damage identification during the long-term monitoring. In the real ambient condition, the temperature change results in the variation of dynamic responses since it affects to material properties and boundary conditions (Park *et al.* 1999, Kim *et al.* 2003, Sohn 2007, Sim *et al.* 2014, Huynh *et al.* 2015a). The temperature change also affects the properties of the piezoelectric sensor. Both the dielectric constant and the coupling constant of the sensor vary proportionally with the temperature. Also, Young's modulus and dimensions of the piezoelectric sensor are dependent on the temperature (Woon and Mitchell 1996, Hooker 1998). According to Liang *et al.* (1994), the EMI response is a function of the dynamic properties of the host structure and the piezoelectric properties of the sensor. Therefore, it is evident that the temperature change would result in the change in the EMI response.

In recent years, the impedance-based technique has been applied for detecting the prestress-loss occurrence in the prestressed anchorage (Nguyen and Kim 2012, Huynh *et al.* 2015b, Min *et al.* 2016, Huynh and Kim 2017a). Several researchers have studied the effect of temperature on the EMI response measured from the tendon-anchorage of prestressed concrete girder (PSC) (Kim *et al.* 2010, Park *et al.* 2015). Due to the non-uniform thermal behaviors among the structural components of the PSC girder (e.g., concrete girder, steel tendon, and anchorage), the temperature change not only causes a relatively slight variation in the prestressing force (Kim *et al.* 2013, Huynh and Kim 2017b)

*Corresponding author, Professor
E-mail: idis@pknu.ac.kr

^a Post-doctoral Researcher

^b Ph.D. Student

but also modifies stress fields of the anchorage zone, resulting in significant shifts in the EMI signals. In real ambient conditions, the temperature effect could cause false detection of prestress-loss if it is not sufficiently compensated.

Many research attempts have been conducted to develop temperature-effect compensation algorithms tailored to the impedance-based technique. By taking advantage that the temperature-induced variation in the EMI signal is dominated by horizontal shifts of impedance peaks, Koo *et al.* (2009) proposed a maximum cross-correlation (CC) index to avoid the false damage detection from the temperature effect. The method is simple to perform but the frequency band used in the compensation process should be sufficiently narrow and carefully selected (Fabricio *et al.* 2014). Sepehry *et al.* (2011) used the artificial neural network (ANN)-based algorithm to minimize false alarms caused by temperature change and varying load. The method requires a large number of training dataset obtained from a wide range of environmental and operational conditions. Thus, the false damage detection can be occurred when untrained patterns are used for the temperature compensation (Huynh and Kim 2018).

Principal component analysis (PCA) has been regarded as a simple and nonparametric statistical technique which is used to emerge the variation and bring out the strong patterns in a high-dimensional data. Recently, the PCA has been applied in several impedance-based SHM problems since the PCA-based method requires simple computation process so that it is suitable for long-term and real-time impedance-based SHM. To reduce the amount of data analysis and avoid unwanted noises, Park *et al.* (2008) used the PCA to extract only essential information of the raw EMI responses. However, the method by Park *et al.* (2008) was experimentally evaluated for impedance monitoring of a bolted connection under the unwanted noises that were not caused by temperature variations. Koo *et al.* (2008) proposed a simple PCA-based strategy to filter only meaningful frequency shifts caused by damage as the temperature-free damage indicator for the impedance-based technique. In many cases, however, the frequency shift is not an effective damage-sensitive indicator because the structural damage also causes variation in the EMI magnitude. To better quantify the damage severity, Min *et al.* (2015) modified Koo's strategy by using the damage indices instead of the frequency shift. Lim *et al.* (2011) proposed the data normalization technique based on kernel PCA to eliminate the temperature effects. However, the accuracy of the method by Lim *et al.* (2011) is quite dependent on an appropriate design of damage-sensitive features and the amount of collected impedance data.

In this study, a simple PCA-based temperature filtering algorithm is proposed for the EMI-based tendon force monitoring of prestressed tendon anchorages. First, the EMI monitoring via a piezoelectric interface device is designed for prestress-loss detection in a tendon anchorage system. Next, the PCA-based temperature filtering algorithm is developed tailored for the EMI monitoring of the prestressed tendon anchorage. To establish the PCA-based filter model, the proposed algorithm utilizes damage-

sensitive features obtained from sub-ranges of the EMI data. Finally, the proposed PCA-based algorithm is experimentally evaluated for the prestress-loss detection in a 6.4 m PSC girder under the temperature-varying condition. To evaluate the performance and effectiveness of the proposed algorithm, the prestress-loss detection results before and after using the PCA-based temperature filtering are discussed with respect to two different EMI features.

2. PZT Interface-based tendon force monitoring method

2.1 EMI monitoring via PZT interface

In EMI monitoring practices, sensitive frequency bands are often unknown and usually identified by try-and-error (Park *et al.* 2003). In many cases, the measured frequency bands can be higher than 100 kHz to sensitively capture incipient damage in structures (Chaudhry *et al.* 1995, Soh *et al.* 2000, Park *et al.* 2003, Kim *et al.* 2010). This causes the difficulty for the implementation of low-cost EMI sensing devices which allow frequency ranges below 100 kHz (Nguyen and Kim 2012, Ho *et al.* 2012, Hong *et al.* 2012, Park *et al.* 2015). To overcome this limitation, Huynh and Kim (2014) proposed a PZT interface method that can acquire EMI responses sensitive to structural properties at predetermined frequency bands less than 100 kHz. The method uses an interfacial structure equipped with a piezoelectric sensor to indirectly acquire the impedance data from a target structure. The geometry and material properties of the interface structure should be appropriately designed so that the resonant responses occur below 100 kHz (Huynh and Kim 2017a).

As schematized in Fig. 1, the PZT interface-based method is adopted to monitor EMI responses of a prestressed tendon anchorage with predetermined sensitive frequency bands less than 100 kHz. The interface device is an aluminium beam which has a flexible section in the middle and two bonded sections. As shown in Fig. 1, the PZT interface is surface-mounted on the bearing plate of prestressed tendon anchorage. The flexible section, where the PZT sensor is installed, is intentionally designed to make the PZT patch freely vibrate below 100 kHz when being mounted on the host structure. The main advantage of this PZT interface prototype lies in its portability which allows it being easily mounted on and detached from the host structure's surface.

To obtain the EMI signatures, an impedance analyzer is used to simultaneously excite the PZT sensor on the interface by a harmonic voltage $V(\omega)$, see Fig. 1. The output harmonic current $I(\omega)$ is then measured and the ratio between $V(\omega)$ and $I(\omega)$ is defined as the EMI $Z(\omega)$, in which the structural mechanical impedance (SMI) of the PZT sensor $Z_a(\omega)$ and the host structure $Z_s(\omega)$ (i.e., interface-anchorage system) are coupled together (Liang *et al.* 1994), as follows

$$Z(\omega) = \frac{V}{I} = \left\{ i\omega \frac{w_a l_a}{t_a} \left[\hat{\epsilon}_{33}^T - \frac{1}{Z_a(\omega)/Z_s(\omega) + 1} d_{33}^2 \hat{Y}_{xx}^E \right] \right\}^{-1} \quad (1)$$

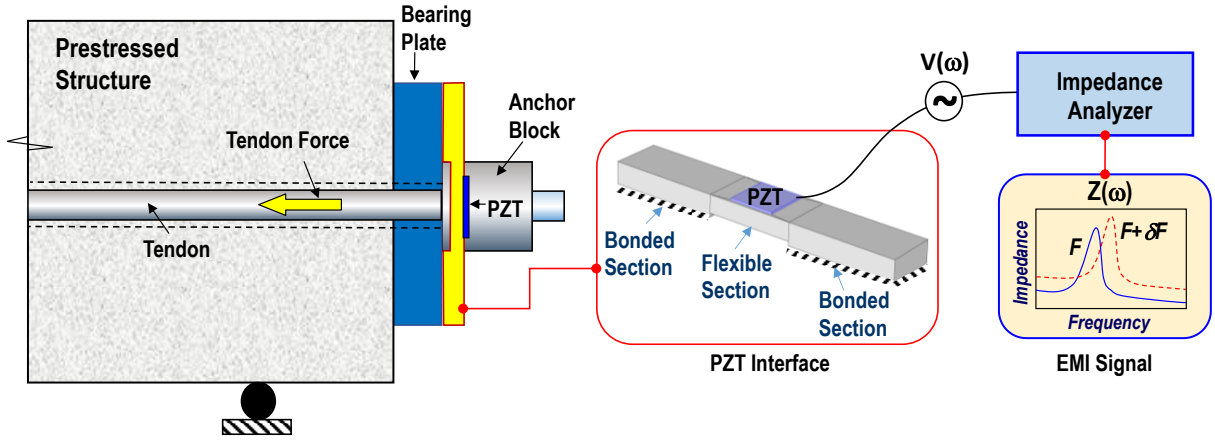


Fig. 1 EMI monitoring via PZT interface for prestressed tendon anchorage

where $\hat{Y}_{xx}^E = (1 + i\eta)Y_{xx}^E$ is the complex Young's modulus of the PZT patch at zero electric field; $\hat{\epsilon}_{xx}^T = (1 - i\delta)\epsilon_{xx}^T$ is the complex dielectric constant at zero stress; d_{3x} is the piezoelectric coupling constant in the x -direction at zero stress; and w_a , l_a , and t_a are the width, length, and thickness of the PZT patch, respectively. The parameters η and δ are structural damping loss factor and dielectric loss factor of piezoelectric material, respectively.

2.2 Prestress-loss monitoring using PZT interface's EMI responses

Fig. 2 illustrates the PZT interface-anchorage interacting system when the PZT sensor on the interface is excited by a harmonic voltage. According to the contact mechanism, the prestressing effect of the tendon force can be represented by spring (i.e., k_1^c , k_2^c) and dashpot (i.e., c_1^c , c_2^c) at the contact interfaces between the bearing plate and the prestressed structure and between the anchor block with the bearing plate (Johnson 1985). The interface structure is simplified by spring, dashpot, and mass (i.e., k^i , c^i , m^i) at the PZT driving point.

When the prestress force is changed, the stress field of the bearing plate and the contact parameters of the tendon anchorage are altered. These variations would modify the SMI $Z_s(\omega)$ of the interface-anchorage system and then lead to the change of the EMI response $Z(\omega)$, according to Eq. (1). As the result, the variation of prestress forces can be detected via quantifying the variation in EMI responses which are measured via the PZT interface mounted on the tendon anchorage. Huynh and Kim (2017a) proposed an analytical impedance model of the PZT interface-anchorage system to theoretically demonstrate the feasibility of the PZT interface technique.

The change of EMI responses can be quantified by common impedance features such as root-mean-square-deviation (RMSD) or cross-correlation-deviation (CCD). The CCD index can be computed as follows (Zagrai and Giurgiutiu 2001)

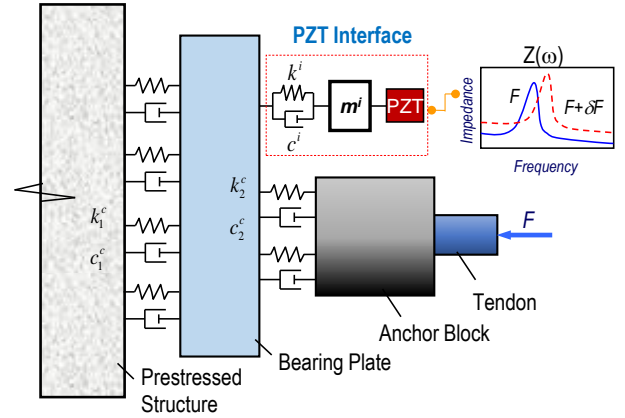


Fig. 2 PZT interface-anchorage interacting system

$$\text{CCD} = 1 - \frac{1}{\sigma_z \sigma_z^*} E \left\{ \left[\frac{\text{Re}(Z(\omega_i)) - \text{Re}(\bar{Z})}{\text{Re}(Z^*(\omega_i)) - \text{Re}(\bar{Z}^*)} \right] \times \right\} \quad (2)$$

where $E[\cdot]$ is the expectation operation; $Z(\omega_i)$ and $Z^*(\omega_i)$, signify the impedance at the i^{th} frequency before and after damage, respectively; \bar{Z} and \bar{Z}^* indicate the mean values of $Z(\omega_i)$ and $Z^*(\omega_i)$, respectively; σ_z and σ_z^* are the standard deviation values of $Z(\omega_i)$ and $Z^*(\omega_i)$, respectively. Also, the RMSD index can be obtained by (Sun *et al.* 1995)

$$\text{RMSD} = \sqrt{\frac{\sum_{i=1}^N [Z^*(\omega_i) - Z(\omega_i)]^2}{\sum_{i=1}^N [Z(\omega_i)]^2}} \quad (3)$$

where N denotes the number of swept frequencies. It is noted that the RMSD index is sensitive to both the vertical shift (i.e., magnitude change) and the horizontal shift (i.e., frequency shift) of the EMI signatures while the CCD index is mainly sensitive to the horizontal shift.

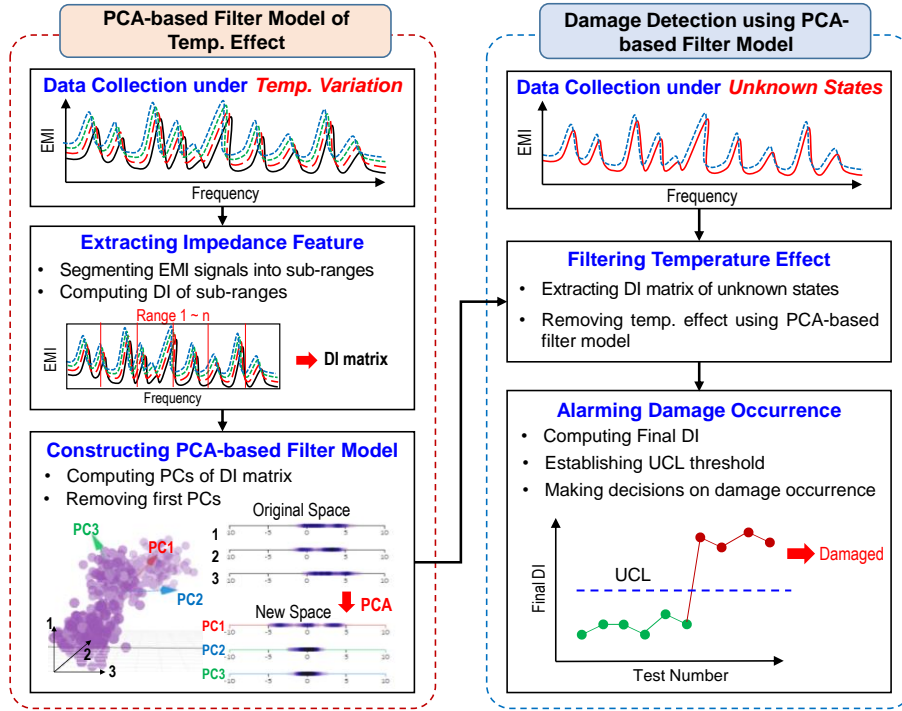


Fig. 3 PCA-based filtering procedure for EMI-based damage detection

3. PCA-based temperature effect filtering algorithm

3.1 PCA-based filter model

The PCA technique linearly transforms the original dataset of variables into a substantially smaller one of uncorrelated variables, which can describe most of the information of the original dataset (Jlooffe 1986). In this study, the linear PCA technique is applied to identify the principal components (PCs) of the damage indices which are computed using sub-frequency ranges of collected EMI signals. Since each resonant EMI peak has the distinct nature under the temperature change, there exist several EMI peaks which vary more significantly than others (Huynh and Kim 2016). By searching the governing trends of the temperature-induced variation in the damage-sensitive features (i.e., RMSD and CCD) of the sub-frequency ranges, the temperature effects could be filtered out via the processes of data compression and feature extraction.

To develop the PCA model, it is important to arrange the computed damage indices (i.e., RMSD and CCD) in a matrix form $[DI]_{m \times n}$ which contains the damage indices of n resonant frequency ranges and m EMI samples. When the matrix $[DI]$ is obtained, the covariance matrix $[C]$ can be constructed, as follows

$$[C] = \frac{1}{m-1} [DI]^T [DI] \quad (4)$$

where the covariance matrix $[C]_{n \times n}$ is a square symmetric $n \times n$ matrix that measures the degree of linear relationships within the matrix $[DI]$. The subspaces in the PCA are defined by decomposing the covariance matrix, as follows

$$[C] = [A][\Lambda][A]^T \quad (5)$$

where $[A]$ is the matrix whose columns are the eigenvectors, and $[\Lambda]$ is the diagonal matrix whose diagonal terms are the eigenvalues. The columns of $[A]$ are sorted according to the eigenvalues by descending order. This process gives the PCs of the original dataset in order of significance.

By selecting only r first PCs which describe most of the variability in the dataset, a reduced transformation matrix $[A_R]$ is obtained. Then, the original dataset $[DI]$ can be geometrically transformed to the new matrix $[Z]$ which describes the projection of $[DI]$ over the orientations of the PCs, as follows

$$[Z] = [DI][A_R] \quad (6)$$

In case of using full PCs $[A]$, the original data can be invertible as $[DI] = [Z][A]^T$. In the case of using reduced PCs $[A_R]$, with the given $[Z]$, the original data can be partially recovered by projecting the matrix $[Z]$ back onto the original n -dimensional space, as follows

$$[DI_R] = [Z][A_R]^T = [DI][A_R][A_R]^T \quad (7)$$

If the r PCs are removed, the residual matrix of the damage indices, $[DI_E]$ can be obtained by subtracting the original data $[DI]$ to the projected data $[DI_R]$, as follows

$$[DI_E] = [DI] - [DI_R] = [DI]([I] - [A_R][A_R]^T) \quad (8)$$

Since only a few first PCs govern most of the variability in the damage indices, the residual matrix $[DI_E]$ in Eq. (8) contain the damage indices after compensating the

temperature effects. In Eq. (8), the term $([I] - [A_E] [A_E]^{-1})$ is referred as the PCA-based filter model. It should be noted the proposed model reduces the impedance feature space while the kernel PCA model by Lim *et al.* (2011) increases the dimensionality of original feature data.

To account for n resonant peaks, a final damage index (Final DI_i) for the i^{th} impedance measurement is formed by averaging the damage indices of n sub-ranges as

$$\text{Final } DI_i = \frac{1}{n} \sum_{j=1}^n DI_{Eij} \quad (9)$$

To classify abnormal events, an alarming threshold known as upper control limit (UCL) is established using the final damage index under the intact state (Hong *et al.* 2012), as follows

$$\text{UCL} = \mu + 3\sigma \quad (10)$$

where μ and σ are respectively the mean and the standard deviation of the final damage index under the intact state. Note that the UCL determined by three standard deviations of the mean has a confidence level of 99.7%.

As compared to previous studies adopted the PCA algorithm (Park *et al.* 2008, Lim *et al.* 2011), the proposed method eliminates temperature effects with a different manner, via establishing a PCA-based filter model. Also, the proposed method has a simple computational procedure. To construct a PCA-based filter model, the well-known damage-sensitive feature (RMSD or CCD) is extracted from different sub-frequency ranges of impedance signals. Meanwhile, in the method by Lim *et al.* (2011), various damage-sensitive features should be carefully designed.

3.2 PCA-based filtering algorithm for EMI-based damage detection

The PCA-based temperature filter algorithm for the EMI-based damage detection is schematized in Fig. 3. It consists of two parts: (1) PCA-based filter model of temperature effect and (2) damage detection using PCA-based filter model.

In the first part, the PCA-based filter model is constructed in the three steps. Firstly, the EMI samples are measured at various temperatures under the intact state of the host structure. Secondly, the EMI signals are segmented into sub-ranges and the damage index of the sub-ranges is computed using Eqs. (2) and (3). Then, the damage index matrix is constructed. Finally, the PCs of the damage index matrix are identified using Eq. (5) and the first PCs are removed. Then, the PCA-based model for filtering the temperature effect is established using Eq. (8).

In the second part, the damage detection process using the PCA-based filter model is performed in three steps. Firstly, the EMI samples are measured at the unknown states of the host structure. Secondly, the damage index matrix is computed for the unknown states using Eqs. (2) and (3). Then, the PCA-based filter model is applied to remove the temperature effect from the damage index of the unknown states using Eq. (8). Finally, the final damage index is computed using Eq. (9). For the decision-making,

the threshold UCL is calculated using Eq. (10). If the final damage index is over the UCL, the damage occurrence is alerted; otherwise, there is no damage occurrence.

4. Experimental evaluation on PSC girder

4.1 EMI measurement under temperature variation and tendon-force change

4.1.1 Test-setup of PSC girder

Laboratory experiments were performed on a post-tensioned PSC girder. As schematized in Fig. 4(a), the PSC girder of 6.4 m long was simply supported by two steel bars with two overhangs of 0.2 m long. The concrete has a 28-day compressive strength of 23.6 MPa and the mass density of approximately 2400 kg/m³. A 7-wire mono-strand $\phi 15.2$ mm was used for the tendon of the PSC girder. The prestress forces were applied to the tendon via a stressing jack installed at one anchorage. A load cell was installed at the same anchorage to measure the applied forces from the stressing jack. The cross-section of the girder is detailed in Fig. 4(b). At the anchorage zone shown in Fig. 4(c), an aluminium PZT interface was attached to the bearing plate, near the anchor block. The aluminium interface was designed with the length of 100 mm (flexible beam section was 30 mm and two outer contacting bodies were 35 mm each), the width of 33 mm, the flexible section's thickness of 4 mm, and the contacting section's thickness of 5 mm. A PZT-5A patch sized 20x20x0.51 mm³ was installed in the middle of the interface device. It's worth noting that the specification of the PZT interface was selected based on its natural frequencies to predefine sensitive frequency ranges of EMI responses below 100 kHz, which is the allowable frequency range of wireless impedance sensing technology (Mascarenas *et al.* 2007, Park *et al.* 2010, and Park *et al.* 2015).

Fig. 5 shows test-setup of the PSC girder in the laboratory. For the installation, two mounted sections of the PZT interface was bonded to the bearing plate using surface insensitive instant adhesive Loctite 401. For recording the temperature, a K-type thermocouple wire was set up on the top surface of the PSC girder, as zoomed in Fig. 5. Low-power excitation, 1V harmonic voltage, was used to excite the PZT interface to acquire the EMI signal. To ensure an accurate quantification of the temperature effect, the EMI response was measured by a wired high-performance HIOKI 3532 analyser. The frequency range considered in this study was 10-50 kHz. This is because the frequency range higher than 50 kHz contained weak impedance signals (Huynh and Kim 2017a). Kyowa EDX-100A data logger was used to acquire temperature from the thermocouple wire. The sampling rate of 1 Hz was set for the temperature measurement during the tests.

4.1.2 Simulation of temperature-varying condition and tendon-force change

The EMI monitoring at the tendon-anchorage was performed in the laboratory (Pukyong National University,

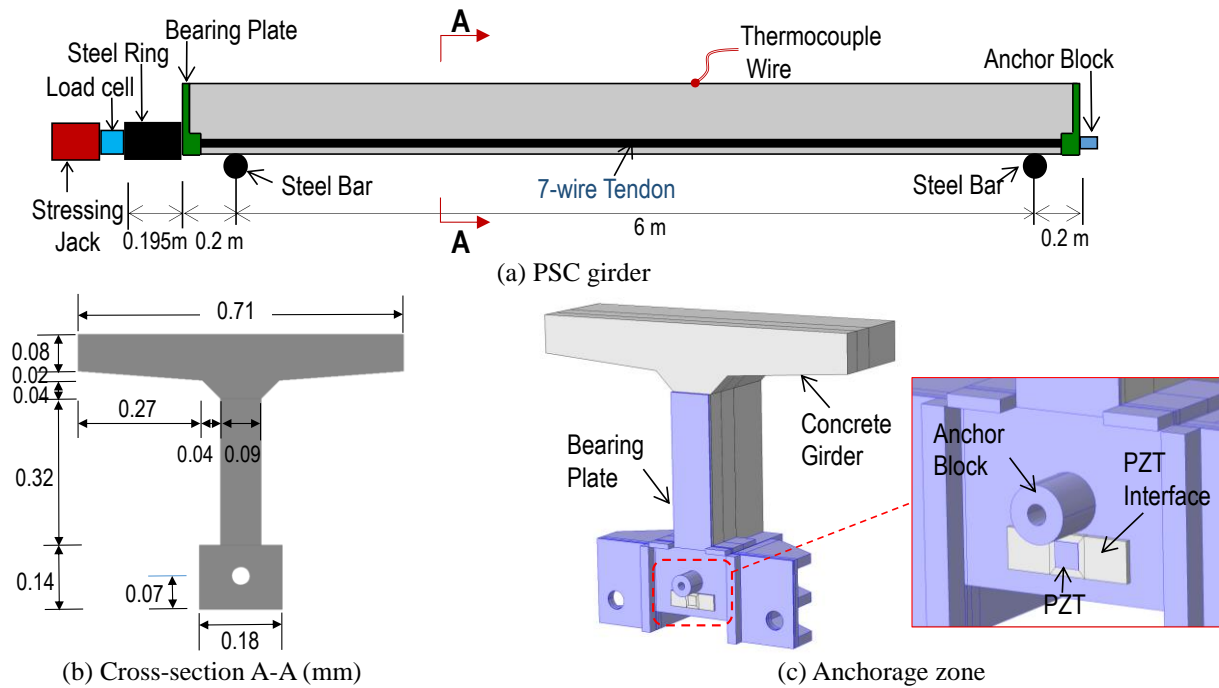


Fig. 4 Schematic of PSC girder

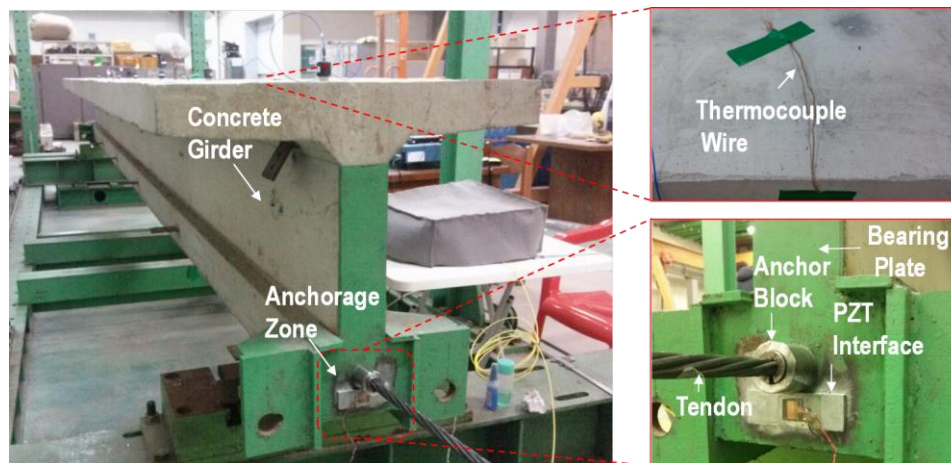


Fig. 5 Test-setup of PSC girder in laboratory

Korea) for two continuous test scenarios: temperature-varying tests and prestress-loss tests. For the temperature-varying tests, to analyze the temperature effect, the temperature was changed between 6.72~22.33°C while the tendon force was set as 138.3 kN (PS1) at the temperature 22.33°C. The room temperature was firstly heated up to 22.33°C by using four heaters located at the four edges of the room. After reaching the temperature 22.33°C, the heaters were turned off to let the room temperature change gradually between 6.72~22.33 °C according to the ambient temperature to minimize the error caused by the non-uniform temperature distribution. It is shown from Fig. 6 that the room temperature gradually changed between daytime and nighttime during about 5 days monitoring. The impedance analyzer was set for periodical auto-monitoring every 10 min with the scanning frequency range of 10-50

kHz in which EMI responses were measured for 901 points (50 Hz frequency interval). Total 669 tests (Tests 1-669) were conducted on the PSC girder under the varying temperature condition.

For the prestress-loss tests, it is supposed that the prestress-loss occurred at a particular temperature. Thus, the tendon force was reduced to 128.5 kN (PS2), 117.7 kN (PS3), 108.9 kN (PS4), and 99.1 kN (PS5) at temperatures near 19°C. The EMI responses of the PZT interface were measured for analyzing the prestress force effect and detecting the prestress-loss. Five sets of EMI signatures were sampled for each prestress-force level. Totally, 25 tests (Tests 670-694) were acquired from the PZT interface under the near-constant temperature.

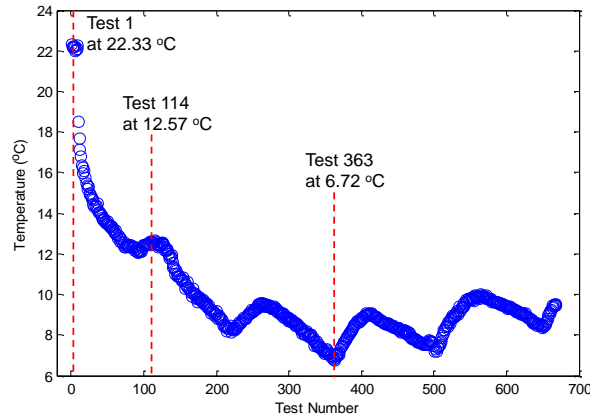


Fig. 6 Temperature variation and prestress-loss simulated in the laboratory

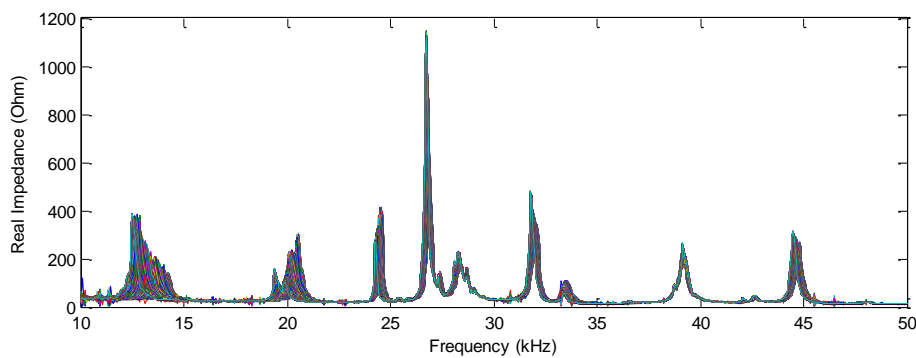


Fig. 7 EMI signals of 10-50 kHz under temperatures 6.72-22.33°C and PS1

4.1.3 EMI responses vs temperature and tendon force

As shown in Fig. 7, total 669 EMI samples were obtained for the temperature variation 6.72-22.33°C. The tendon force was the intact condition (i.e., PS1) and the signals were measured in 10-50 kHz from the PZT interface. From the figure, several resonant peaks were observed in the frequency range and those peaks reflect the considerable contribution of the EMI to the overall EMI response. It is shown that the temperature change modified the EMI signatures. The frequency and magnitude of EMI peaks varied significantly with the temperature.

The variation of the resonant EMI peaks was analyzed and plotted in temperature-frequency diagrams, as shown in Fig. 8. For most resonant peaks, the resonant frequencies went up as the temperature was increased, as observed in Figs. 8(a)-8(d) and 8(f). Only the resonant peak in 37-41 kHz experienced a slight frequency decrement, as shown in Fig. 8(e). It is shown that the bandwidth of some EMI peaks was also changed with the temperature, implying the variation in the modal damping of the PZT interface-anchorage system.

As shown in Fig. 9, the EMI signatures were obtained for the healthy state PS1 and four prestress-loss cases PS2-PS5. The temperature was kept about 19°C and the signals were also measured in 10-50 kHz from the PZT interface. As depicted in Fig. 9, the frequencies and magnitudes of the EMI peaks were changed with the prestressing force.

As plotted in Fig. 10, the prestress force-frequency responses were analyzed to observe the change in peak frequencies induced by the variation of prestressing force. When the prestress force was reduced from 138.3 kN (PS1) to 99.1 kN (PS5), the frequency of EMI peaks went down, revealing the decrement in the modal stiffness of the PZT interface-tendon anchorage system. The bandwidth of some EMI peaks was also changed with the prestressing force, indicating the variation in the modal damping of the PZT interface-anchorage system.

4.2 Temperature-filtered tendon force monitoring

4.2.1 Tendon force monitoring using PCA-based algorithm and CCD index

Once the EMI signals were measured from the PZT interface, the frequency range of 10-50 kHz was first divided into 7 narrow sub-ranges with the same frequency interval of 5 kHz. As indicated in Fig. 11, they are Range 1 of 11-16 kHz, Range 2 of 16-21 kHz, Range 3 of 21-26 kHz, Range 4 of 26-31 kHz, Range 5 of 31-36 kHz, Range 6 of 36-41 kHz and Range 7 of 41-46 kHz. The frequency interval was determined so that each sub-range contains one significant resonant EMI peak. By using the EMI signal of Test 114 at 12.63°C (near the mean of the temperature variation) as the reference, the damage indices (i.e., RMSD and CCD) were computed for these 7 sub-ranges.

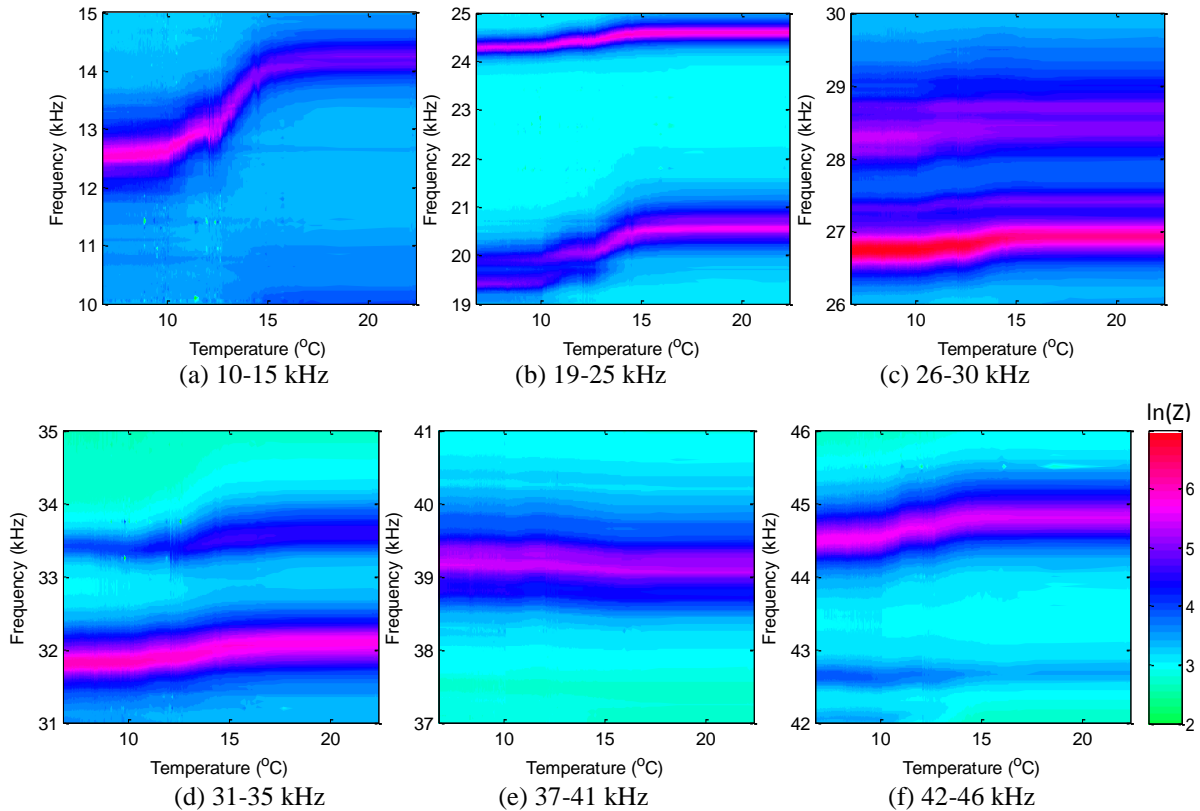


Fig. 8 Variation of resonant EMI peaks with temperature

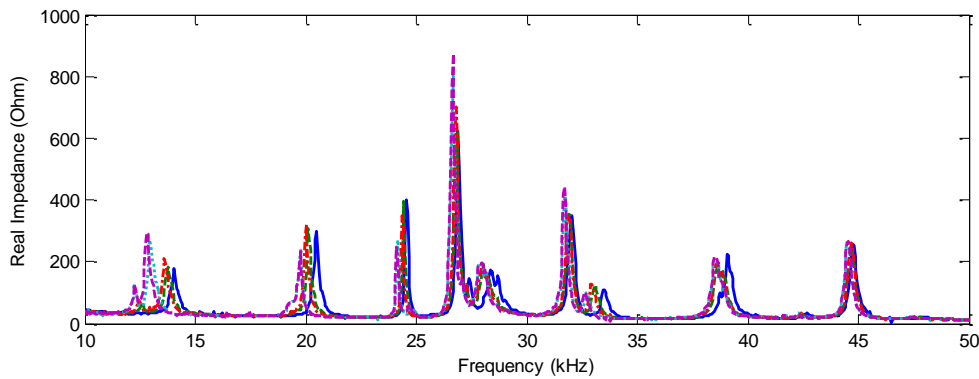


Fig. 9 EMI signal of 10-50 kHz under PS1-PS5 and temperature near 19°C

In reality, the ambient temperature often follows a normal distribution and varies around a mean value. The reference temperature near the mean value could enhance the accuracy of temperature filtering.

The matrix $[CCD]_{669 \times 7}$ that contains the CCD values of the 7 ranges for Tests 1-669 (under temperature variation 6.72-22.33°C and PS1) was constructed. The PCs of the CCD matrix were computed and the original CCD data was transformed into the new coordinate system which shows the best view of the data's variation. As plotted in Fig. 12(a), the new space consists of 7 dimensions: PC1 - PC7. The PCA transformation ensures that the axis PC1 has the most variation, the axis PC2 is the second-most, and the axis PC7

is the least. As shown in Fig. 12(b), the variance of the PCs revealed that the PC1 and PC2 contributed the largest to the temperature-induced variation in the CCD data. Therefore, the PCA-based filter model was established by removing the PC1 and PC2.

For tendon force monitoring in the PSC girder, the matrix $[CCD]_{25 \times 7}$ that contains the CCD values of the 7 ranges for Tests 670-694 (under prestress-loss PS1-PS5 and temperature near 19°C) was established. Fig. 13(a) shows the original CCD index of the 7 ranges (before the PCA) for all 694 EMI samples (Tests 1-694) under the temperature variation and prestress-loss events. And, Fig. 13(b) shows the average CCD index of the 7 ranges for all samples.

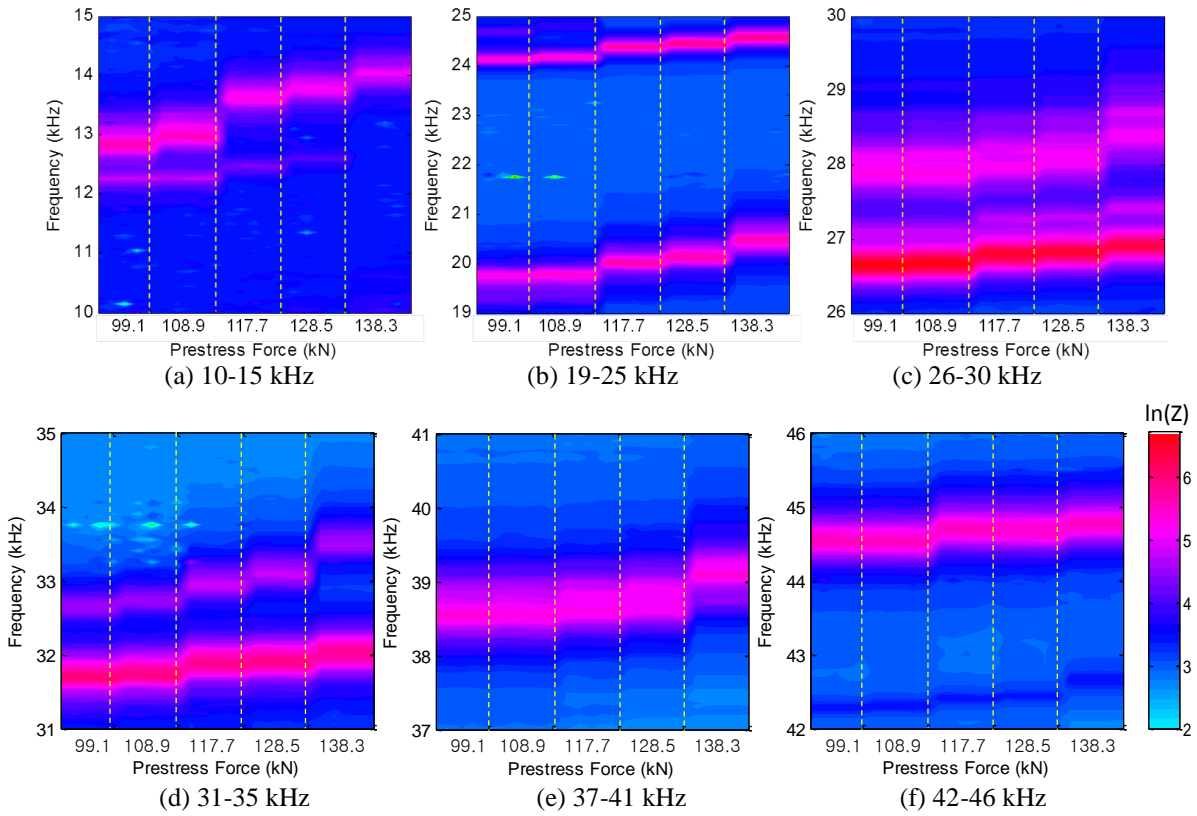


Fig. 10 Variation of resonant EMI peaks with prestressing force

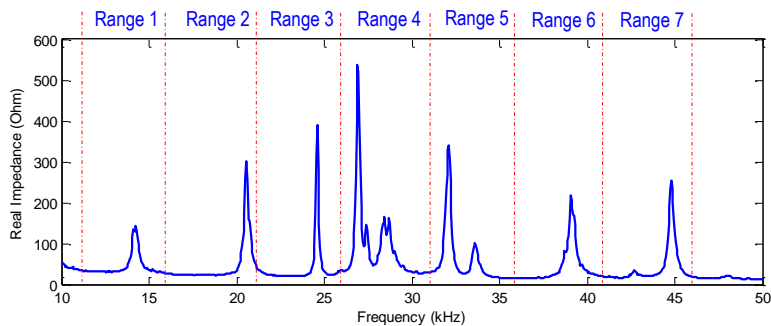


Fig. 11 Seven sub-ranges of EMI used to construct PCA model

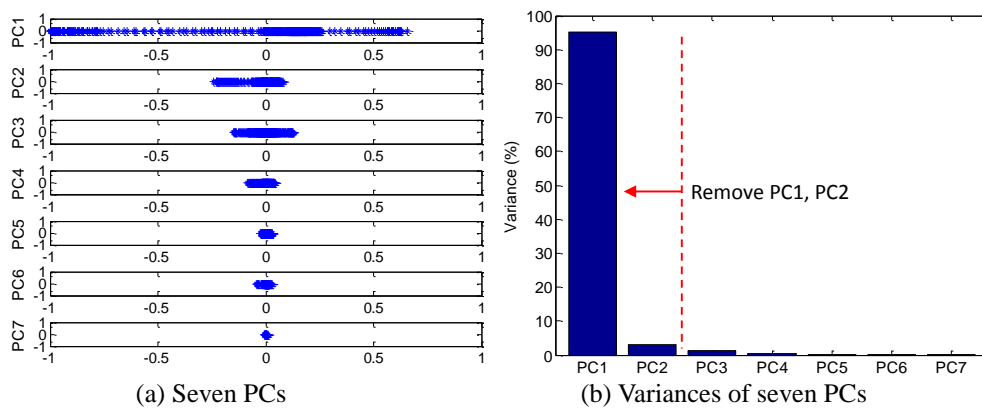


Fig. 12 Principal components of CCD index and their variances

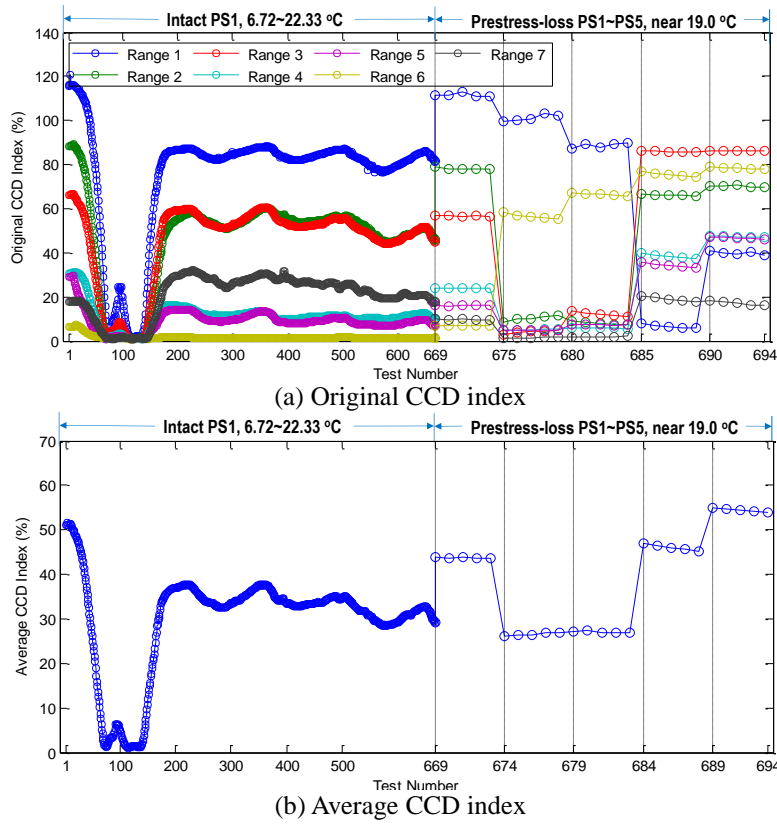


Fig. 13 CCD index of 7 frequency ranges before filtering temperature effect

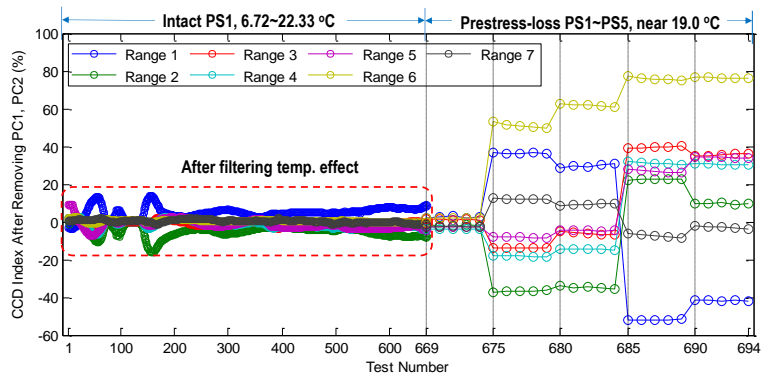


Fig. 14 CCD index of 7 frequency ranges after PCA-based temperature filtering

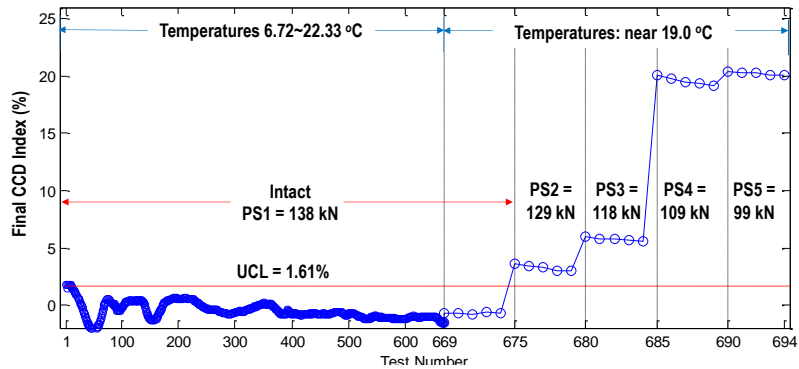


Fig. 15 Tendon force monitoring in PSC girder after PCA-based temperature filtering for CCD index

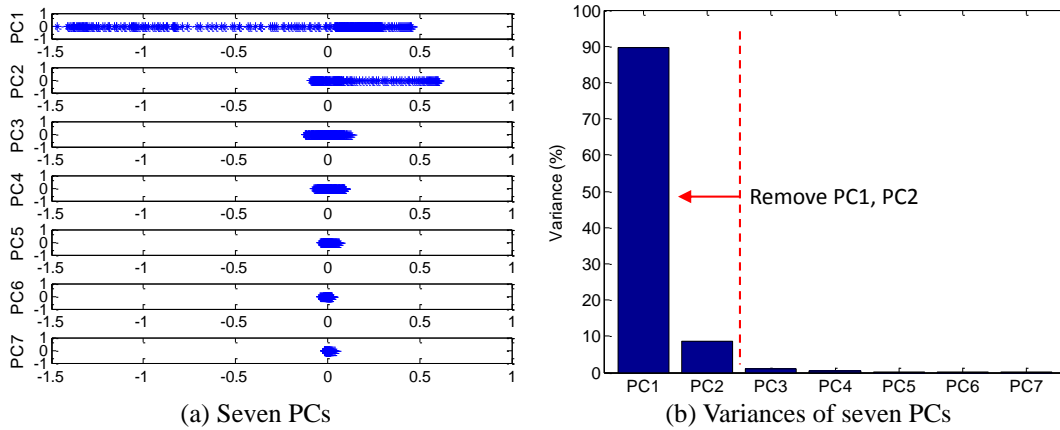


Fig. 16 Principal components of RMSD index under temperature variation

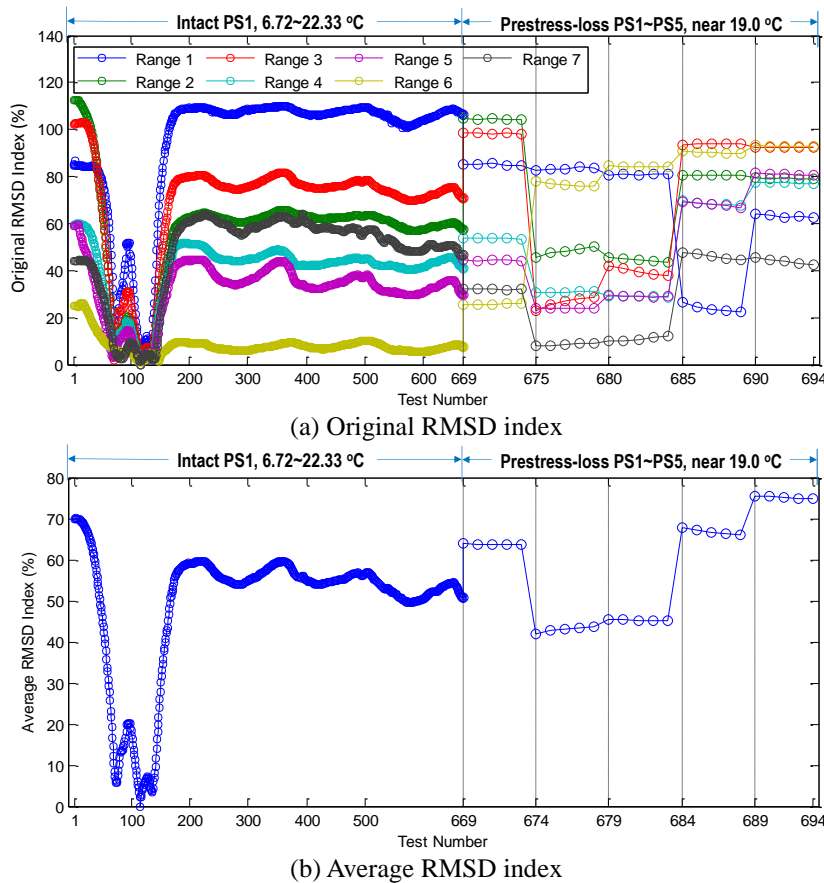


Fig. 17 RMSD index of 7 frequency ranges before filtering temperature effect

The damage indices were plotted in a row of test orders. As illustrated in these figures, it is hard to make a decision for the prestress-loss diagnosis by using the original/average CCD index since the CCD values for the intact and prestress-loss tests were comparable.

Fig. 14 illustrates the CCD index of the 7 ranges after the PCA-based filtering of the temperature effect. By comparing Fig. 14 with Fig. 13, it can be seen that the CCD magnitude of Ranges 1-7 for the intact state was significantly reduced after filtering the temperature effect.

The final CCD index was computed to consider the contribution of all resonant EMI peaks, as shown in Fig. 15. For decision-making on the prestress-loss occurrence in the PSC girder, the UCL threshold was computed using the final CCD index under the intact state (Tests 1-669). The UCL value of 1.61% revealed that the temperature effect was well-filtered by the PCA-based algorithm. As observed from Fig. 15, the final CCD index was below the threshold before the prestress-loss occurrence (Tests 1-674) but above the threshold when the tendon force was reduced (Tests

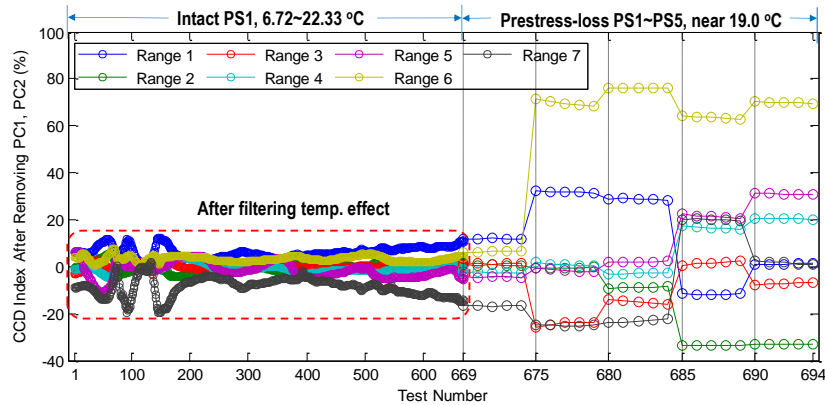


Fig. 18 RMSD index of 7 frequency ranges after PCA-based temperature filtering

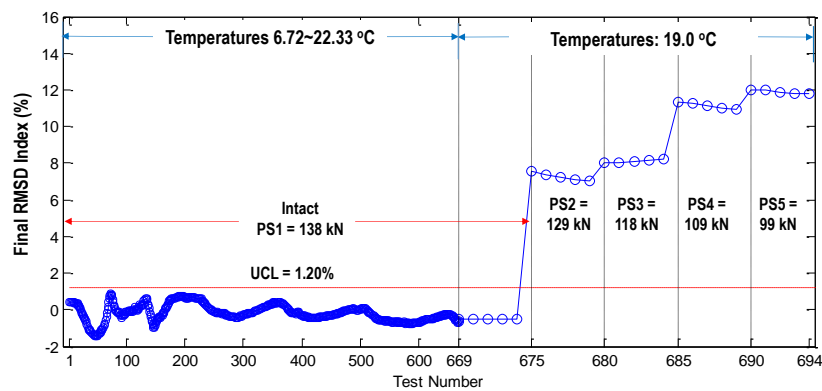


Fig. 19 Tendon force monitoring in PSC girder after PCA-based temperature filtering for RMSD index

675-694). The final CCD index was increased when the damage severity went up. Conclusively, the tendon force change in the PSC girder was successfully detected after filtering the temperature effect out of the CCD index.

4.2.2 Tendon force monitoring using PCA-based algorithm and RMSD index

The tendon force monitoring using RMSD index was also conducted. The matrix $[RMSD]_{669 \times 7}$ that contains the RMSD values of the 7 ranges for Tests 1-669 (under temperature variation 6.72-22.33°C and PS1) was constructed. The PCs of the RMSD matrix were computed.

As plotted in Fig. 16(a), the PC1 and PC2 of the RMSD index exhibited the most variations while the PC7 experienced the least. The variance of the PCs also demonstrated the significant contribution of the PC1 and PC2 to the temperature-induced changes in the RMSD index, see Fig. 16(b). Therefore, the PC1 and PC2 were removed when establishing the PCA-based filter model.

For prestress-loss detection, the RMSD values of the 7 ranges for Tests 670-694 (under prestress-loss PS1-PS5 and temperature near 19°C) was computed and the corresponding matrix $[RMSD]_{25 \times 7}$ was constructed. For all 694 EMI samples (Tests 1-694) under the temperature variation and prestress-loss events, the original RMSD index (before the PCA) of the 7 frequency ranges was

plotted in Fig. 17(a). The average RMSD index of the 7 ranges for all samples were computed accordingly, as plotted in Fig. 17(b). As observed in these figures, the variations of the original/average RMSD index caused by temperature variation (i.e., 6.72-22.33°C) were comparable with those caused by the prestress-loss events (i.e., PS1-PS5) and it is difficult to distinguish the prestress-loss occurrence in the PSC girder.

After the PCA-based filtering of the temperature effect, the RMSD index of the 7 ranges was plotted in Fig. 18. By comparing with Fig. 17(a), Fig. 18 showed that the RMSD magnitude for the intact state was significantly reduced after filtering the temperature effect. To consider the contribution of all resonant EMI peaks, the final RMSD index was calculated, as depicted in Fig. 19. By using the final RMSD index under the intact state (Tests 1-669), the UCL threshold was obtained as 1.20%. The ignorable UCL value revealed that the temperature effect was sufficiently filtered by the proposed PCA-based algorithm. It can be seen from Fig. 19 that the prestress-loss events in the PSC girder were clearly distinguished. Before the prestress-loss occurrence (Tests 1-674), the final RMSD index was below the threshold but it was sharply above the threshold when the prestress-loss occurred in the PSC girder (Tests 675-694). It is also observed that the final RMSD index was increased along with the prestress-loss severity.

Conclusively, the prestress force variation in the test structure was successfully alarmed after filtering the temperature effect out of the RMSD index.

For the damage quantification, the major difference between the CCD and the RMSD indices is that the RMSD index quantifies both the horizontal and vertical shifts in the signal while the CCD index is mainly dependent on the horizontal shift in the EMI signal. As observed from Figs. 7-10, the effects of temperature variation and tendon-force change caused both horizontal and vertical shifts in the EMI signatures. This means that the temperature effect could be more sufficiently filtered when employing the RMSD index to feed the PCA-based algorithm than the CCD index. By comparing Fig. 19 with Fig. 15, it is found that the RMSD index after the PCA was better in the indication of small prestress-loss levels (i.e., PS2-PS3) than the CCD index.

5. Conclusions

In this study, a simple PCA-based temperature filter model was proposed for the PZT interface-based EMI monitoring in PSC girders under temperature-varying condition. Firstly, the PZT interface-based tendon force monitoring method was presented for the prestressed tendon anchorage. Next, the PCA-based temperature filtering algorithm was outlined tailored to the EMI monitoring of the prestressed tendon anchorage. The proposed algorithm utilized the well-known damage-sensitive feature obtained from sub-ranges of the EMI data to establish the PCA-based filter model. Finally, the PCA-based algorithm was successfully evaluated for distinguishing the prestress-loss events in a real 6.4 m PSC girder under the temperature variation. The prestress-loss detection results before and after using the PCA-based temperature filtering were discussed with respect to the different EMI features.

As compared with the previous studies, the uniqueness of this paper lies in: (1) This study proposed a PCA-based temperature filtering algorithm tailored for the PZT interface-based prestress-loss monitoring in tendon-anchorage systems; (2) The proposed method eliminated temperature effects with a different manner, via establishing a PCA-based filter model; (3) The proposed method has a simple computational procedure. To construct a PCA-based filter model, well-known EMI features are extracted from different sub-frequency ranges of impedance data; (4) This study examined two different common EMI features (RMSD and CCD indices) for the PCA-based temperature filtering problem and showed that to more sufficiently filter the temperature effects the RMSD index should be used to feed the PCA model.

As a future work, a larger temperature range and more realistic temperature tests (i.e., ambient temperature variation) should be examined to sufficiently investigate the relationship between the EMI response and the temperature.

Acknowledgements

This research was supported by a grant (18CTAP-

C142999-01) from Technology Advancement Research Program (TARP) funded by Ministry of Land, Infrastructure and Transport of Korean government.

References

- Ayres, J.W., Lalonde, F., Chaudhry, Z. and Rogers, C.A. (1998), "Qualitative impedance-based health monitoring of civil infrastructures", *Smart Mater. Struct.*, **7**, 599-605.
- Chaudhry, Z., Joseph, T., Sun, F. and Rogers, C. (1995), "Local-area health monitoring of aircraft via piezoelectric actuator/sensor patches", *Smart Structures and Integrated Systems, Proceedings of the SPIE*, **2443**, San Diego, CA.
- Fabricio G.B., Danilo E.B., Vinicius A.D.A. and Jose A.C.U. (2014), "An experimental study on the effect of temperature on piezoelectric sensors for impedance-based structural health monitoring", *Sensors*, **14**, 1208-1227.
- Ho, D.D., Lee, P.Y., Nguyen, K.D., Hong, D.S., Lee, S.Y., Kim, J.T., Shin, S.W., Yun, C.B. and Shinozuka, M. (2012), "Solar-powered multi-scale sensor node on Imote2 platform for hybrid SHM in cable-stayed bridge", *Smart Struct. Syst.*, **9**(2), 145-164.
- Ho, D.D., Ngo, T.M. and Kim, J.T. (2014), "Impedance-based damage monitoring of steel column connection: numerical simulation", *Struct. Monit. Maint.*, **1**(3), 339-356.
- Ho, D.D., Nguyen, K.D., Yoon, H.S. and Kim, J.T. (2012), "Multiscale acceleration-dynamic strain-impedance sensor system for structural health monitoring", *Int. J. Distrib. Sens. N.*, **2012**, 1-17.
- Hong, D.S., Nguyen, K.D., Lee, I.C. and Kim, J.T. (2012), "Temperature-compensated damage monitoring by using wireless acceleration-impedance sensor nodes in steel girder connection", *Int. J. Distrib. Sens. N.*, **2012**, 1-12.
- Hooker, M.W. (1998), "Properties of PZT-based piezoelectric ceramics between -150 and 250°C", *Technical Report NASA/CR-1998-208708*, NASA, USA
- Hu, X., Zhu, H. and Wang, D. (2014), "A study of concrete slab damage detection based on the electromechanical impedance method", *Sensors*, **14**, 19897-19909.
- Huynh, T.C. and Kim, J.T. (2014), "Impedance-based cable force monitoring in tendon-anchorage using portable PZT-interface technique", *Math. Probl. Eng.*, **2014**, 1-11.
- Huynh, T.C. and Kim, J.T. (2016), "Compensation of temperature effect on impedance responses of PZT interface for prestress-loss monitoring in PSC girders", *Smart Struct. Syst.*, **17**(6), 881-901.
- Huynh, T.C. and Kim, J.T. (2017a), "Quantitative damage identification in tendon anchorage via PZT interface-based impedance monitoring technique", *Smart Struct. Syst.*, **20**(2), 181-195.
- Huynh, T.C. and Kim, J.T. (2017b), "FOS-based prestress force monitoring and temperature effect on unbonded tendon of PSC girder", *J. Aerosp. Eng.*, **30**(2), 1-14.
- Huynh, T.C. and Kim, J.T. (2018), "RBFN-based temperature compensation method for impedance monitoring in prestressed tendon anchorage", *Struct. Control Health Monit.*, **25**(6), e2173.
- Huynh, T.C., Dang, N.L. and Kim, J.T. (2017), "Advances and challenges in impedance-based structural health monitoring", *Struct. Monit. Maint.*, **4**(4), 301-329.
- Huynh, T.C., Park, Y.H., Park, J.H., Hong, D.S. and Kim, J.T. (2015a), "Effect of temperature variation on vibration monitoring of prestressed concrete girders", *Shock Vib.*, **2015**, 1-9.
- Huynh, T.C., Park, Y.H., Park, J.H. and Kim, J.T. (2015b), "Feasibility verification of mountable PZT-interface for impedance monitoring in tendon-anchorage", *Shock Vib.*, **2015**,

- 1-11.
- Jloioffe, I.T. (1986), *Principal Component Analysis*, Springer, New York.
- Johnson, K.L. (1985), *Contact Mechanics*, Cambridge University Press, Cambridge.
- Kim, J.T., Nguyen, K.D. and Huynh, T.C. (2013), "Wireless health monitoring of stay cable using piezoelectric strain response and smart skin technique", *Smart Struct. Syst.*, **12**(3-4), 381-397.
- Kim, J.T., Park, J.H., Hong, D.S. and Park, W.S. (2010), "Hybrid health monitoring of prestressed concrete girder bridges by sequential vibration-impedance approaches", *Eng. Struct.*, **32**, 115-128.
- Kim, J.T., Huynh, T.C. and Lee, S.Y. (2014), "Wireless structural health monitoring of stay cables under two consecutive typhoons", *Struct. Monit. Maint.*, **1**(1), 47-67."
- Kim, J.T., Yun, C.B. and Yi, J.H. (2003), "Temperature effects on frequency-based damage detection in plate-girder bridges", *J. KSCE*, **7**(6), 725-733.
- Koo, K.Y., Park, S., Lee, J.J. and Yun, C.B. (2009), "Automated impedance-based structural health monitoring incorporating effective frequency shift for compensating temperature effects", *J. Intel. Mat. Syst. Str.*, **20**, 367-377.
- Koo, K.Y., Park, S., Lee, J.J. and Yun, C.B. (2008), "Temperature effects-free impedance-based structural health monitoring using principal component analysis", *Proceedings of IMAC-XXVI: Conference & Exposition on Structural Dynamics*, 1-6.
- Liang, C., Sun, F.P. and Rogers, C.A. (1994), "Coupled electro-mechanical analysis of adaptive material - Determination of the actuator power consumption and system energy transfer", *J. Intel. Mat. Syst. Str.*, **5**, 12-20.
- Lim, H.J., Kim, M.K., Sohn, H. and Park, C.Y. (2011), "Impedance-based damage detection under varying temperature and loading conditions", *NDT&E Int.*, **44**, 740-750.
- Mascarenas, D., Todd, M.D., Park, G. and Farrar, C.R. (2007), "Development of an impedance-based wireless sensor node for structural health monitoring", *Smart Mater. Struct.*, **16**(6), 2137-2145.
- Min, J., Shim, H., Yun, C.B. and Hong, J.W. (2016), "An electromechanical impedance-based method for tensile force estimation and damage diagnosis of post-tensioning systems", *Smart Struct. Syst.*, **17**(1), 107-122.
- Min, J., Yi, J.H. and Yun, C.B. (2015), "Electromechanical impedance-based long-term SHM for jacket-type tidal current power plant structure", *Smart Struct. Syst.*, **15**(2), 283-297.
- Nguyen, K.D. and Kim, J.T. (2012), "Smart PZT-interface for wireless impedance-based prestress-loss monitoring in tendon-anchorage connection", *Smart Struct. Syst.*, **9**(6), 489-504.
- Nguyen, T.C., Huynh, T.C., Yi, J.H. and Kim, J.T. (2017), "Hybrid bolt-loosening detection in wind turbine tower structures by vibration and impedance responses", *Wind Struct.*, **24**(4), 385-403.
- Park, G., Kabeya, K., Cudney, H. and Inman, D. (1999), "Impedance-based structural health monitoring for temperature varying applications", *JSME International Journal Series A Solid Mechanics and Material Engineering*, **42**, 249-258.
- Park, G., Sohn, H., Farrar, C. and Inman, D. (2003), "Overview of piezoelectric impedance-based health monitoring and path forward", *Shock Vib. Digest*, **35**(6), 451-463.
- Park, J.H., Huynh, T.C. and Kim, J.T. (2015), "Temperature effect on wireless impedance monitoring in tendon anchorage of prestressed concrete girder", *Smart Struct. Syst.*, **15**(4), 1159-1175.
- Park, J.H., Kim, J.T., Hong, D.S., Mascarenas, D. and Lynch, J.P. (2010), "Autonomous smart sensor nodes for global and local damage detection of prestressed concrete bridges based on accelerations and impedance measurements", *Smart Struct. Syst.*, **6**(5), 711-730.
- Park, S., Lee, J.J. and Yun, C.B. (2008), "Electro-mechanical impedance-based wireless structural health monitoring using PCA-data compression and k-means clustering algorithms", *J. Intel. Mat. Syst. Str.*, **19**(4), 509-520.
- Ryu, J.Y., Huynh, T.C. and Kim, J.T. (2017), "Experimental investigation of magnetic-mount PZT interface for impedance-based damage detection in steel girder connection", *Struct. Monit. Maint.*, **4**(3), 237-253.
- Sepehry, N., Shamsirsaz, M. and Abdollahi, F. (2011), "Temperature variation effect compensation in impedance-based structural health monitoring using neural networks", *J. Intel. Mat. Syst. Str.*, **20**(10), 1-8.
- Sim, S.H., Li, J., Jo, H., Park, J.W., Cho, S., Spencer Jr, B.F. and Jung, H.J. (2014), "A wireless smart sensor network for automated monitoring of cable tension", *Smart Mater. Struct.*, **23**, 1-10.
- Soh, C.K., Tseng, K.K., Bhalla, S. and Gupta, A. (2000), "Performance of smart piezoceramic patches in health monitoring of a RC bridge", *Smart Mater. Struct.*, **9**, 533-542.
- Soh, C.K., Yang, Y. and Bhalla, S. (2012), *Smart Materials in Structural Health Monitoring, Control and Biomechanics*, Springer-Verlag Berlin Heidelberg
- Sohn, H. (2007), "Effects of environmental and operational variability on structural health monitoring", *Philosophical Transactions of the Royal Society A*, **365**, 539-560.
- Sun, F.P., Chaudhry Z., Liang, C. and Rogers C.A. (1995), "Truss structure integrity identification using PZT sensor-actuator", *J. Intel. Mat. Syst. Str.*, **6**, 134-139.
- Wang, D., Wang, Q., Wang, H. and Zhu H. (2016), "Experimental study on damage detection in timber specimens based on an electromechanical impedance technique and RMSD-based Mahalanobis distance", *Sensors*, 1-17.
- Woon, C.E. and Mitchell, L.D. (1996), "Variations in structural dynamic characteristics caused by changes in ambient temperature: Part I. Experimental", *Proceeding of the 14th IMAC, SEM*.
- Yang, Y., Annamdas, V.G.M., Wang, C. and Zhou, Y. (2008), "Application of multiplexed FBG and PZT impedance sensors for health monitoring of rocks", *Sensors*, **8**, 271-289.
- Zagrai, A.N. and Giurgiutiu, V. (2001), "Electro-mechanical impedance method for crack detection in thin plates", *J. Intel. Mat. Syst. Str.*, **12**, 709-718.
- Zahedi, F. and Huang, H. (2017), "Time-frequency analysis of electromechanical impedance (EMI) signature for physics-based damage detections using piezoelectric wafer active sensor (PWAS)", *Smart Mater. Struct.*, **26**, 1-9.

CC